Biosensors and Bioelectronics 77 (2016) 790–798

Contents lists available at ScienceDirect

Biosensors and Bioelectronics

journal homepage: www.elsevier.com/locate/bios

Label-free biomolecular detection at electrically displaced liquid interfaces using interfacial electrokinetic transduction (IET)

Nicholas Mavrogiannis [a], Francesca Crivellari [a], Zachary R. Gagnon [b,*]

[a] Johns Hopkins University, 3400 North Charles Street, Maryland Hall 221 C, Baltimore, MD 21218, United States of America
[b] Johns Hopkins University, 3400 North Charles Street, Maryland Hall 220 A, Baltimore, MD 21218, United States of America

ARTICLE INFO

Article history:
Received 25 August 2015
Received in revised form
6 October 2015
Accepted 14 October 2015
Available online 23 October 2015

Keywords:
Microfluidics
Electrokinetics
Biosensing
Dielectrophoresis
Interfacial polarization

ABSTRACT

Biosensors require a biorecognition element that specifically binds to a target analyte, and a signal transducer, which converts this targeted binding event into a measurable signal. While current biosensing methods are capable of sensitively detecting a variety of target analytes in a laboratory setting, there are inherent difficulties in developing low-cost portable biosensors for point-of-care diagnostics using traditional optical, mass, or electroanalytical-based signal transducers. It is therefore important to develop new biosensing transducer elements for recognizing binding events at low cost and in portable environments. Here, we demonstrate a novel electrokinetic liquid biosensing method for the sensitive label-free detection of a model biomolecule against a background of serum protein. The biosensor is based on the motion of a microfluidic-generated electrical liquid interface when subjected to an external alternating current electrical field. We demonstrate that the electric field-induced motion of the interface can be used as a sensitive and specific transducer for the detection of avidin at femtomolar concentrations in solution. This new detection strategy does not require surface functionalization or fluorescent labels, and has the potential to serve as a sensitive low-cost method for portable biomarker detection.

1. Introduction

Biosensors combine targeted biological recognition with physicochemical transduction to detect specific biomolecules within a biological sample. They are used in a wide range of analytical applications, including diagnosis and treatment of infectious diseases, biowarfare detection (Peruski et al., 2002; Peruski and Peruski, 2003), environmental monitoring (Palchetti and Mascini, 2008; Rebe Raz and Haasnoot, 2011), drug discovery (Cooper and Cooper, 2002; Myszka and Rich, 2000), cell biology (Lee et al., 2008; Roelse et al., 2013), cancer research (Voura et al., 2004; Wang, 2006) and point-of-care diagnostic testing (Wan et al., 2013; Watkins et al., 2013). Here, we address a key challenge to developing label-free homogenous biosensors for sensitive biomolecular detection and kinetic analysis using microfluidic biosensing systems that normally require fluorescently labeled biomolecules and optical quantification.

Combining biosensors with microfluidic transducers can fulfill an increasing demand for fast, inexpensive sensors capable of molecular detection and analysis. Microfluidic biosensors provide several advantages over traditional laboratory-based detection methods, including faster analysis time, reduced sample and reagent consumption, and potential automation with sample processing units using on-chip microfluidic valves (Yoo et al., 2008), pumps, mixers (Lin et al., 2013) and detectors. In microfluidics, liquid transport usually occurs at low Reynolds number where the fluid flow is laminar; fluid streams flow side-by-side and mixing is driven only by diffusion (Kamholz et al., 1999; Ismagilov et al., 2000; Hatch et al., 2004).

Microfluidic liquid interfaces have been used as homogenous biosensing substrates for quantitative molecular detection and kinetic analysis in solution phase. The interface is created using laminar flow, where two streams combine at a fluidic junction and flow side-by-side down a main channel. One stream has a target probe and the second stream contains the biological sample of interest (Atencia and Beebe, 2005; Hatch et al., 2001). Biorecognition occurs in solution phase as the target and sample streams diffusively mix at their contacting liquid interface where target and sample molecules specifically bind to one another. This approach offers an inexpensive, yet extremely powerful method for biosensing and biomolecular kinetic analysis, and has been used to quantify fast kinetic processes, extract kinetic rate constants, perform sensitive on-chip immunoassays and detect DNA hybridization reactions in solution.

To create a complete biosensor, the microfluidic interface is coupled with a transducing element to convert recognition events into a detectable measurement signal. Depending on the nature of

* Corresponding author.

http://dx.doi.org/10.1016/j.bios.2015.10.045
0956-5663/

the transduced biosensor signal, detection can be performed optically (Pollet et al., 2009), electrically (Rodriguez et al., 2005; Coltro et al., 2014) or mechanically (Ariyaratne and Zocchi, 2015). Biosensing at microfluidic liquid interfaces, however, is currently only performed using optical methods such as fluorescent microscopy, fluorescence energy transfer (FRET) (Cao et al., 2012), fluorescence correlation spectroscopy (Dong and Ren, 2014), confocal fluorescent microscopy (Yoo et al., 2014), and fluorescence lifetime imaging microscopy (FLIM) (Giraud et al., 2010). While effective, they require fluorescently labeled probe molecules and optical components, which can significantly increase the cost and size of the microfluidic platform.

We report a label-free homogeneous electrokinetic biosensor for detecting and quantifying bioaffinity interactions in solution. Our approach combines continuous microfluidic flow with alternating current (AC) electrokinetics. Electrokinetics integrates well with microfluidics and is a useful tool for a variety of on-chip fluidic applications including cell manipulation (Gagnon et al., 2010a, 2010b), liquid mixing (Lee et al., 2001), particle trapping (Gagnon et al., 2010a, 2010b) and fluidic routing (Fu et al., 2015). In our electrokinetic approach, depicted in Fig. 1, bioaffinity binding occurs at a microfluidic liquid interface. We create the interface using a microfluidic T-channel device with two fluid inlets and a single fluidic outlet; two fluids combine at the channel junction and create an interface as they flow side-by-side down the main channel to the outlet (Fig. 1a). An array of microelectrodes is fabricated in the main flow channel and used to deliver a polarizing electric field across the fluid interface. To be polarizable, and capable of being manipulated with the applied electric field, we engineer an electrical mismatch into the interface. In this way, the interface is an electrical interface (EI), comprised of two co-flowing fluid streams with different electrical conductivity (σ) and permittivity (ε). Using the EI as a substrate for biomolecular reaction, two solutions – one containing a target protein and the other containing an analyte probe – are pumped into separate T-channel inlets at a constant flow rate, inter-diffuse across the EI and specifically bind at the liquid interface (Fig. 1b). During this process, an AC electrical field is applied across the EI. Due to the large electrical mismatch, the interface polarizes and electrokinetically displaces across the main flow channel, perpendicular to the main flow direction (Fig. 1c) (Desmond et al., 2012). The magnitude and direction of this displacement is proportional to the electrical mismatch at the EI. Here, we demonstrate that specific biomolecular interactions influence this mismatch, and allow for biomolecular interactions to be detected and quantified without fluorescent labels by measuring the interfacial displacement under an external electric field during binding (Fig. 1c).

Our label-free biosensing method uses the liquid interface as a homogenous substrate for specific binding, and its motion in an AC electric field as the transducer for biomolecular recognition. We therefore propose a new class of biosensors based on interfacial electrokinetic transduction (IET): specific binding changes the electrical properties at the EI, which is electrokinetically transduced and detected by measuring perturbations in field-induced fluid displacement.

In this work, we demonstrate how to use IET to monitor avidin–biotin binding kinetics in real-time without labels. Moreover, the IET biosensor is specific and sensitive, and able to detect as low as 250 femtomolar avidin concentrations against a 5 mg/mL background of bovine serum albumin (BSA). Through this study, we establish a methodology for rapid label-free IET biosensing at electrical liquid interfaces, demonstrate sensor performance and sensitivity for the detection of biomolecules, and measure avidin–biotin binding kinetics with millisecond time resolution. This new electrokinetic sensor can provide a low-cost, rapid, and portable biosensing system for label-free real-time kinetic analysis and on-site biomolecular diagnostics in free solution.

2. Materials and methods

2.1. Microfluidic device fabrication

Experiments were performed using the microfluidic T-channel device shown in Fig. 1a. It was fabricated using standard soft photolithography and microfabrication techniques. First, microchannel electrodes were fabricated using wet chemical etching. Glass cover slips (50×30 mm^2, No. 1, Fisher Scientific) were coated with 2 nm of chromium and 50 nm of gold using electron beam evaporation. The cover slips were patterned with photoresist (Shipley 1813) and exposed metal was etched using gold and chromium etchant creating an array of patterned metal electrodes. The microchannel was fabricated in PDMS (Momentive, RTV 615A). A 10:1 mixture of PDMS elastomer and curing agent was poured atop the wafer and baked at 85 °C for 50 min. The PDMS was gently peeled off the wafer and fluid ports were punched with a 0.75 mm diameter biopsy punch (Ted Pella, Inc.). The PDMS microchannel and electrode pattern were then exposed to oxygen plasma (Jelight, Model 42A) and immediately aligned and sealed under an inverted microscope. As shown in Fig. 1a, the device consists of a main flow channel 100 μM wide and 65 μM high. The

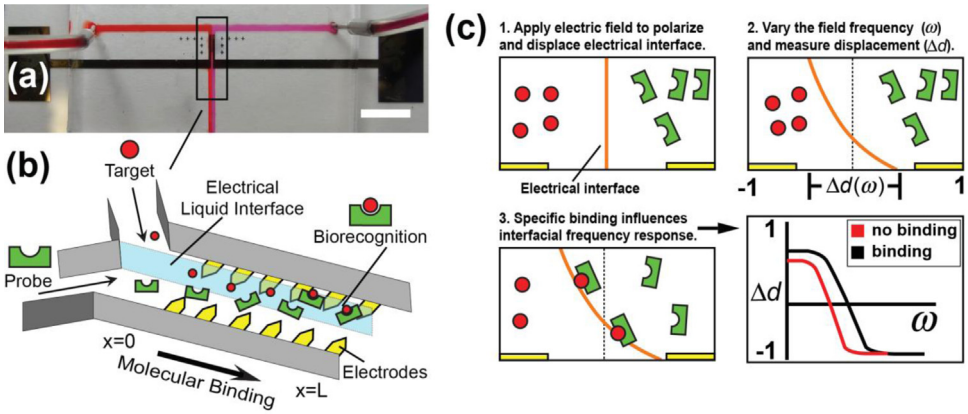

Fig. 1. (A) Microfluidic T-channel device with integrated electrodes used to create an electrical liquid interface for the IET sensor. Scale bar 5.0 mm; (B) schematic illustration of target-probe binding along the liquid interface; and (C) principles of IET sensor operation – (1) specific binding occurs at the electrical interface; (2) an electric field polarizes and displaces the interface a distance Δd, which is a function of the field frequency; (3) binding influences the polarizability of the interface and is detected by measuring interface frequency response at different values of field frequency.

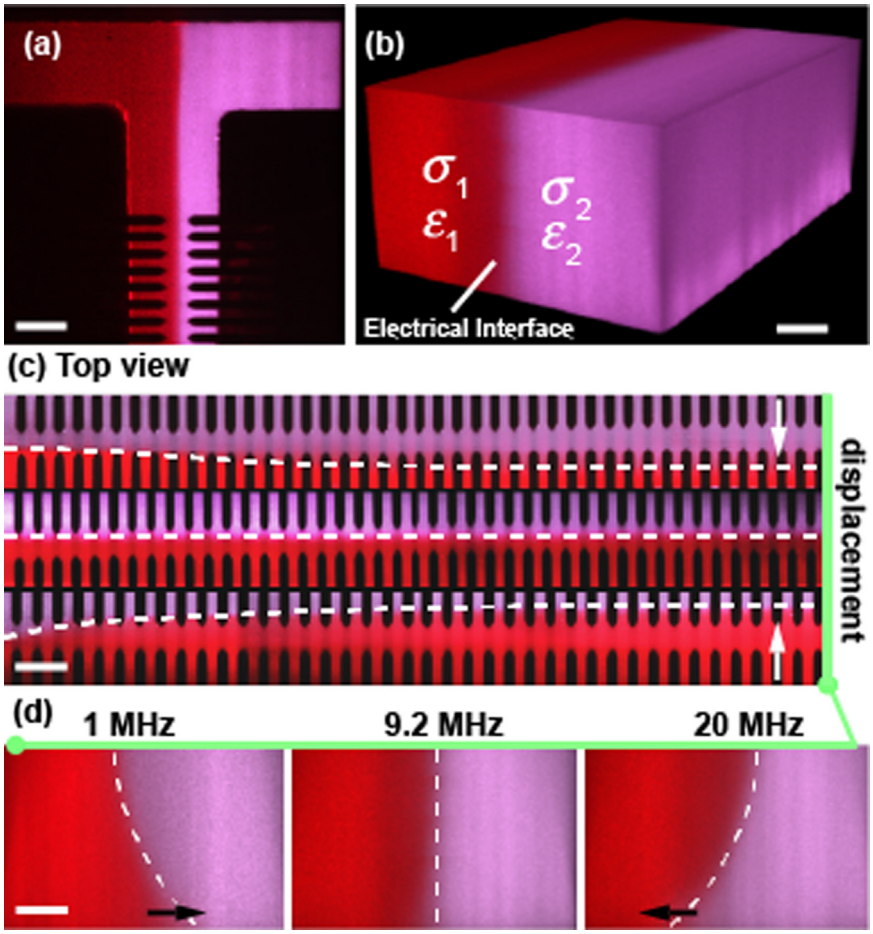

Fig. 2. (A) Confocal micrograph of two fluorescently labeled fluids flowing side-by-side to create a liquid interface. Scale bar 50 μm; (B) 3D confocal image stack of the electrical interface formed between to fluids with different electrical conductivities and dielectric constants. Scale bar 20 μm; (C) the interface enters the electrode array and displaces across the flow channel. The direction of this displacement is dependent on the frequency of the applied electric field. Scale bar 50 μm; and (D) confocal micrograph illustrates a side-view of the interface at different electric field frequencies. Scale bar 20 μm. (For interpretation of the references to color in this figure, the reader is referred to the web version of this article.)

embedded electrodes are axially separated by 20 μM and symmetrically bridge the channel width with a total length of 2.0 mm. Electrodes with sharp points are utilized in order to maximize the electric field strength across the liquid interface, as the sharp point serves to focus the electric field to the tip of the electrode.

2.2. Sensor measurement

The electrical interface was created using the microfluidic "T-channel". Two fluid streams were introduced into the device via pressure driven flow using an externally pressurized cryogenic vial. Shown in Fig. 2a, the left-most (red) high conductivity stream consists of a 0.5 M phosphate buffered saline, pH 7.4, (PBS) solution with 10 ng/mL of Alexa Fluor 594 (Invitrogen). The right-most (purple) high dielectric stream consists of 0.8 M 6-aminohexanoic acid (Sigma-Aldrich) (AHA) labeled with 10 ng/mL of Alexa Fluor 647 (Invitrogen). AHA is a water-soluble zwitterion used for increasing the dielectric constant of aqueous solution. Prior to fluorescent labeling, the AHA solution is spun down in a centrifuge for 15 min in 1 g/mL Dowex MR-3 (Sigma) ion exchange resin to remove trace salts and reduce solution conductivity (Mavrogiannis et al., 2015). A cross-sectional view of the resulting fluid interface was imaged using dual excitation confocal microscopy (Fig. 2b).

To create the electrical interface two fluid streams, each with a different set of electrical properties, are pressure injected into the microfluidic device. An AC potential of 10 V peak-to-peak (V_{pp}) at a frequency of 1 MHz was dropped across the electrodes, and slowly is increased to 20 MHz while continuously monitoring the displaced position of the fluid interface.

2.3. Protein solutions

Biotin, avidin, bovine serum albumin, and mouse anti-bovine serum albumin were purchased from Sigma Aldrich, USA, and used as received. A 16 μM biotin solution was made by diluting a 4 mM stock with AHA and labeled with 10 ng/ml Alexa Fluor 594, and pH adjusted to 7.4. The avidin solution was made by adding powdered avidin to PBS labeled with 10 ng/ml Alexa Fluor 647. The conductivity of the PBS solution was adjusted to 0.25 mS/cm using DI water. All subsequent solution avidin concentrations were made by serial dilutions with a stock dilute PBS. The final avidin concentration was calculated using a UV spectrometer (Thermo Scientific Genesys 10S).

2.4. The electrical interface

IET biosensors are bioaffinity sensitized electrical liquid interfaces that electrokinetically displace in response to biomolecular binding. They require both microfluidic and electrokinetic components. The electrical interface is created using a PDMS microfluidic T-channel. An AC electric field is generated using an array of co-planar gold microelectrodes lithographically patterned onto the

surface of a glass slide. The PDMS-electrode assembly is aligned under an optical microscope and plasma bonded to create a complete electro-fluidic device (Fig. 1a). The EI is composed of two co-flowing electrolyte streams. Both streams – streams 1 (left) and 2 (right) – have finite electrical conductivity and permittivity, but one has a greater electrical conductivity and the other a greater electrical permittivity such that $\sigma_1 > \sigma_2$ and $\varepsilon_2 > \varepsilon_1$. Because the streams do not mix except by diffusion, a sharp electrical mismatch is created at their co-flowing interface, which can be polarized (e.g. charged) and displaced across the microchannel using a perpendicular AC electric field.

2.5. Measuring interfacial frequency response

To quantify displacement, the interface position is imaged using confocal microscopy; each stream is labeled with a different fluorescent markers – Alexa Fluor 594 (red) or 647 (purple) – and imaged, yielding top-down 2D (Fig. 2a) and 3D (Fig. 2b) micrographs of the interface and its position within the microchannel. When a perpendicular AC electric field is applied, the interface displaces across the channel in a direction and magnitude dependent on the field frequency (ω). This displacement response can be confocal imaged and quantified from a top-down and side view. Fig. 2c shows a top-view of the EI displacement over the length of the electrode array for three different applied frequencies: $\omega = 1$ MHz, 9.2 MHz, and 20 MHz. At a frequency of 1 MHz (Fig. 2c-bottom), the interface enters the array and continuously displaces across the main flow channel into the high permittivity flow stream. At high frequency (20 MHz), the displacement direction reverses (Fig. 2c-top). At an intermediate crossover frequency (COF) of 9.2 MHz, the interface does not displace in the electric field and remains stationary over the entire length of the array (Fig. 2c-center).

The force driving interface motion is a surface force that exists over the separation length scale between the electrodes in the array. Because this length scale (20 μm) is smaller than the microchannel height (100 μm), field-driven displacement is localized to the bottom of the microchannel. Fluid near the top of the channel is driven in the opposite direction to satisfy conservation of mass, and the interface appears to tilt to the left or right depending on the applied field frequency. Fig. 2d shows the side-view of the displaced tilted interface for each applied field frequency.

In this work, we propose to use the frequency response of the interface as a biosensing transducer for detecting biomolecules at a microfluidic liquid interface. To accomplish this, we measure the net displacement of the EI as a function of applied electric field frequency at the bottom surface of the microchannel. Fig. 3b shows the complete frequency response of the interface calculated from the micrograph experiment presented in Fig. 2. The displacement (Δd) has been rendered non-dimensional over the microchannel width, and varies from -1 to 1. At the COF, the interface does not displace: $\Delta d = 0$. Above and below the COF the displacement is finite and varies in both direction and magnitude

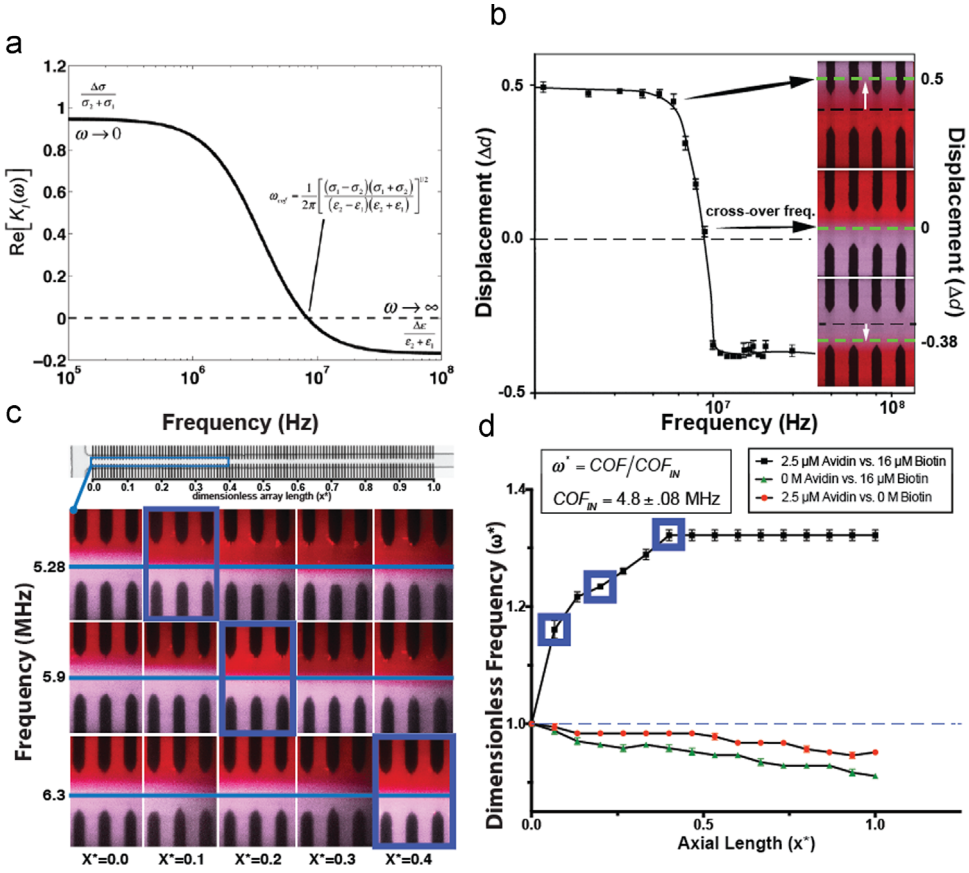

Fig. 3. (A) Liquid interface polarization [Eq. (1)] plotted as a function of field frequency. Low frequency polarization is driven by differences in electrical conductivity, while the interfacial dielectric constant governs the polarization of the interface at high frequency. A cross over frequency [Eq. (2)] is dependent on both interfacial conductivity and dielectric constant. The crossover frequency increases during biomolecular binding. (B) Dimensionless interface displacement measured at different electric field frequencies. An optical micrograph highlights interface position at low (1 MHz), intermediate (9.2 MHz) and high (20 MHz) field frequencies; (C) optical micrographs of the electrical interface captured at different positions and electric field frequencies along the length of the electrode array. The interface crossover for each axial position is highlighted in blue and plotted in the adjacent figure; and (D) IET sensorgram showing the influence of binding on interface crossover frequency plotted against two biosensor negative controls.(For interpretation of the references to color in this figure legend, the reader is referred to the web version of this article.)

with the applied frequency.

2.6. Electrokinetics of an electrical interface-fluidic dielectrophoresis

The motion of an electrical liquid interface in an externally applied AC electric field is known as fluidic dielectrophoresis (fDEP) (Mavrogiannis et al., 2014). Despite being discovered over six decades ago for particle suspensions (Pohl, 1951), dielectrophoresis has only recently been applied to aqueous liquid interfaces. Here, we theoretically define the electrical and frequency dependence on the interface displacement, and apply this to our IET biosensor measurements.

For an EI subjected to a time varying monochromatic AC electric field, the magnitude and direction of the interfacial displacement is directly proportional to the interface polarization factor: $K(\omega)$. This factor describes the magnitude and sign of the field-induced ionic and dielectric charge that is induced at the EI in response to the electric field. Because the field oscillates monochromatically in time, the sign and magnitude of charge at the interface is dynamic, and reverses in phase with the electric field. This process takes a finite time, and depending on the field frequency, not all of the induced charge will be able to dynamically stay in phase. To account for this phase lag, $K(\omega)$ is a complex function with both real and imaginary parts, dependent on field frequency, and liquid conductivity and permittivity differences across the EI. Displacement is driven by the real part of this expression (i.e. interface charging that is in-phase with the applied field). The out of phase (imaginary) part produces a net interfacial electric stress with a zero time-average and does not contribute to interfacial motion. Therefore, we use the real part of the polarization factor in this work.

For an electrical interface composed of two co-flowing aqueous electrolytes with different electrical conductivities and permittivities, the real part of the interfacial polarization factor is

$$Re[K(\omega)] = \frac{(\varepsilon_2 - \varepsilon_1)\tau^2\omega^2}{(\varepsilon_2 + \varepsilon_1)(\tau^2\omega^2+1)} + \frac{(\sigma_2 - \sigma_1)\tau^2\omega^2}{(\sigma_2 + \sigma_1)(\tau^2\omega^2+1)}, \quad (1)$$

where $\tau = \left(\frac{\varepsilon_2+\varepsilon_1}{\sigma_2+\sigma_1}\right)$ is the characteristic charge relaxation timescale at the interface between the two liquids.

Illustrated in Eq. (1), fDEP provides a unique method for quantifying the electrical properties of an EI because displacement direction and magnitude are both dependent on the relative electrical property mismatch between the interface's two co-flowing fluid streams. In Fig. 3a, we plot Eq. (1) as a function of electric field frequency, and highlight the influence of electrical conductivity and permittivity mismatches at high, intermediate, and low AC field frequencies. At low frequency below the COF, polarization is driven by differences in electrical conductivity between the two co-flowing fluids (σ_1–σ_2), which we define here as interfacial conductivity ($\Delta\sigma$). Above the COF at high frequency, displacement is governed solely by interfacial permittivity ($\Delta\varepsilon$). The COF (ω_{COF}) occurs where the net polarization and displacement of the interface is zero (Fig. 3b). It is sensitive to both interfacial conductivity and permittivity, shown here by setting the polarization factor equal to zero ($Re[K(\omega)]=0$), and solving for frequency:

$$\omega_{COF} = \frac{1}{2\pi}\left[\frac{(\sigma_1 - \sigma_2)(\sigma_1 + \sigma_2)}{(\varepsilon_2 - \varepsilon_1)(\varepsilon_2 + \varepsilon_1)}\right]^{\frac{1}{2}} \quad (2)$$

Depicted in Fig. 3a, interface displacement at low and high frequency is influenced only by interfacial conductivity and permittivity, respectively, and the COF is a function of both properties.

The transducing element of our IET biosensor is based on the interface COF. First, because the interface COF is influenced by both EI conductivity and permittivity, it is a single frequency measurement capable of monitoring both of these properties simultaneously at a liquid interface. Second, because the COF occurs when interfacial displacement is zero, it is a simple measurement to observe, and can be made at any axial position along the length of the electrode array.

2.7. Using interfacial crossover frequency to detect specific binding

To detect specific binding at a liquid interface, the EI is sensitized with target probe molecules and forced to flow adjacent to a sample stream containing an analyte. With developed and continuous flow down the T-channel, the fluid at each axial position within the main channel has a different average residence time, and the binding process will be at different time points of diffusive-reactive transport. To monitor binding dynamically during this process, the COF at the EI is quantified at discrete axial positions down the length of the main flow channel. Changes in EI electrical properties during binding influence the COF. Because specific binding progresses forward in time as fluid flows down the length of the array, biomolecular binding can be electrokinetically quantified in time by measuring the COF at varying positions in axial space down the channel length.

3. Results and discussion

3.1. The IET biosensor sensorgram

Our IET biosensor signal was the COF of the liquid interface. We performed this measurement at discrete positions over the entire axial length of the microelectrode array to detect biomolecular binding dynamically in time. We used biotin–avidin as the model system for studying the biosensor response. Avidin binds up to four molecules of biotin with high specificity and affinity, and is a useful binding model for characterizing biosensing systems. To more clearly compare sensor performance against different concentrations of avidin, both experimental variables – the COF and the array position – were rendered dimensionless. Shown in Fig. 3c, the electrode array was rendered dimensionless by its total length (2.0 mm); COF measurements were quantified along a dimensionless axial variable x^*, spanning the domain {0,1}. To maintain consistent reaction residence times within the electrode array, the fluid flow rate was fixed at 5.0 $\frac{\mu L}{min}$. We performed all biosensing experiments using buffers with constant conductivity and permittivity. Because these properties were constant, the COF at $x^*=0$ was fixed: $COF_{IN}=4.8$ MHz $\pm$ 1%. To track the evolution of the COF over the axial position of the array, the COF was rendered dimensionless (ω^*) by COF_{IN} such that $\omega^*=1$ at $x^*=0$.

To determine if specific avidin–biotin binding influences the COF of the interface, a COF sensorgram was captured using 2.5 μM avidin flowing adjacent to 16 μM biotin. We used two negative controls for this experiment – one COF sensorgram was taken without biotin, and a second without avidin. Finally, we measured the COF sensorgram along the EI within the electrode array with both avidin and biotin. Fig. 3d shows the ω^* vs. x^* sensorgram from each experiment. In the absence of binding, the interfacial COF decreases by ~8% over the microchannel length. During avidin–biotin binding, however, the interface COF increases by over 30%, reaching an equilibrium value of $\omega^*=1.3$ at a distance $x^*=0.4$ down the array.

The polarized interface behaves as a biosensor transducer; specific binding influences the interfacial electrical properties, which are transduced electrokinetically as a change in COF for a given position down the electrode array. The COF changes

dynamically, transducing biomolecular binding events over axial length as they proceed forward in time. This concept is reflected in the sensorgram data (Fig. 3d), where the COF appears as a binding curve, increasing over the array length and plateauing as the reaction saturates at the EI. The transduction properties of the EI can be observed optically, as depicted in the confocal micrographs shown in Fig. 3c. As the field frequency is increased, the axial position where no interface displacement occurs shifts. The COF at $x^*=0.1$, for example, is 5.28 MHz; no displacement is observed at this point in the array. This frequency is above COF_{IN} (4.8 MHz) at $x^*=0$ and below the COF for any position where $x^*>0.1$, so the interface deflects in opposing directions surrounding this inflection point. As the applied frequency is increased, the position of the inflection point shifts, corresponding to a new position-dependent COF. These COF inflections are highlighted with blue boxes in Fig. 3c. They represent COF measurements for three axial positions within the electrode array, and correspond to the sensorgram data points emphasized with square boxes in Fig. 3d.

3.2. Avidin–biotin binding influences interfacial conductivity

The response of the IET sensor is based on the influence of bioaffinity binding on the interfacial electrical properties at the EI. Because the COF is sensitive to both interfacial conductivity and permittivity, COF measurements are not enough to determine the exact electrical influence that biomolecular binding has on the interface. To determine how binding influences the electrical properties across the interface, we measured the net displacement during binding over varying AC field frequency at the saturation position $x^*=0.4$ down the electrode array. Fig. 4a shows interfacial displacement spectrum as a function of field frequency for three different avidin concentrations: 0 nM, 25 nM, and 2.5 μM. The electrical mismatch of each of the fluids containing both avidin and biotin were held constant for each experiment. As shown above in Fig. 3a, low frequency displacement is dependent solely on the interfacial conductivity and depends only on interfacial permittivity at high frequency. From the spectra presented in Fig. 4a, avidin–biotin binding influences the low frequency displacement measurements – displacement increases with avidin concentration. At high frequency, however, interfacial displacement remains constant and is not influenced by interfacial binding. Fig. 4b shows a series of confocal micrographs depicting this observation. At 1 MHz the displacement increases as avidin concentration increases (Fig. 4b – Left), and high frequency (20 MHz) displacement remains unaffected with binding (Fig. 4b – Right).

The displacement measurements in Fig. 4 demonstrate that the biomolecular binding of avidin–biotin increases the interfacial conductivity (Δd increases at low frequency with binding), but not alter the interfacial permittivity (Δd remains unaffected at high frequency). While fDEP can give insight as to how the interface is being influenced electrically, it cannot currently provide any mechanistic information about why this increase is occurring. The increase in interfacial conductivity may be due to counter-ion release during binding. One possibility is that a diffuse layer of spatially confined counterions surrounds the charged proteins in solution. During binding, ions are released, which could potentially increase the electrical conductivity in the vicinity of the interface, and produce an increase in COF. Another possibility could be due to a change in electrophoretic mobility due to the negative charge of the bound biotin molecule, which would make the complex a more effective charge carrier at the interface. Currently, however, the precise physical mechanism for the interfacial conductivity increase remains unknown.

3.3. Selective and specific biosensing in a BSA background

Surface-based heterogeneous biosensors can suffer from non-specific adsorption of background proteins, which can reduce sensor sensitivity. The IET sensor utilizes a liquid interface as a biorecognition substrate, and therefore is much less prone to suffer from biofouling or non-specific adsorption of proteins to the sensor surface. However, background interference from non-specific proteins is a major concern when working with real-world clinically relevant samples. To investigate sensor performance in the presence of an abundant background protein, we challenged the sensor with 5 mg/mL of bovine serum albumin (BSA). In order to be able to compare our findings with the avidin–biotin experiments performed without a background (Fig. 3d), the inlet COF and microchannel flow rate were held to less than a 1% deviation from their previous experimental values. Shown in Fig. 5, the COF increases about 25% over the length of the array when taken with 2.5 μM avidin flowing adjacent to 16 μM biotin in the presence of a serum background. To investigate the ability to design specific bioaffinity response into the EI, we removed avidin from the sample stream and replaced it with a 100 nM concentration of anti-BSA. Shown in Fig. 5, the sensor responds to the presence of BSA instead of avidin. Two control experiments were performed to ensure these measurements were specific – removal of anti-BSA and avidin from the sample stream does not produce an increase in the COF along the length of the array.

There are several important features to note regarding the sensor performance depicted in Fig. 5. First, as shown, when compared to the sensorgram without BSA, the selectivity of the sensor towards avidin in the presence of serum decreases by ~30%. This decrease could be due to several factors. There is a possibility that non-specific charge–charge interactions

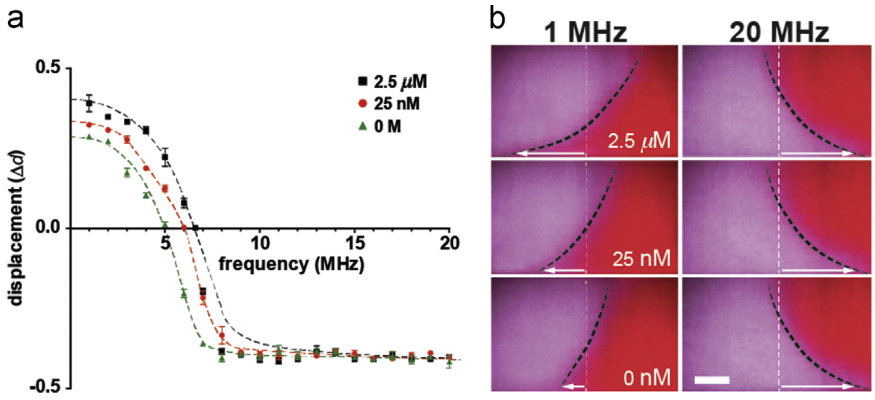

Fig. 4. (A) Interface displacement measured over increasing concentrations of avidin: 0 M, 25 nM, and 2.5 μM. (B) Confocal micrographs illustrate interface position at low (1 MHz) and high (20 MHz) for increasing avidin concentrations. Scale bar 20 μm.

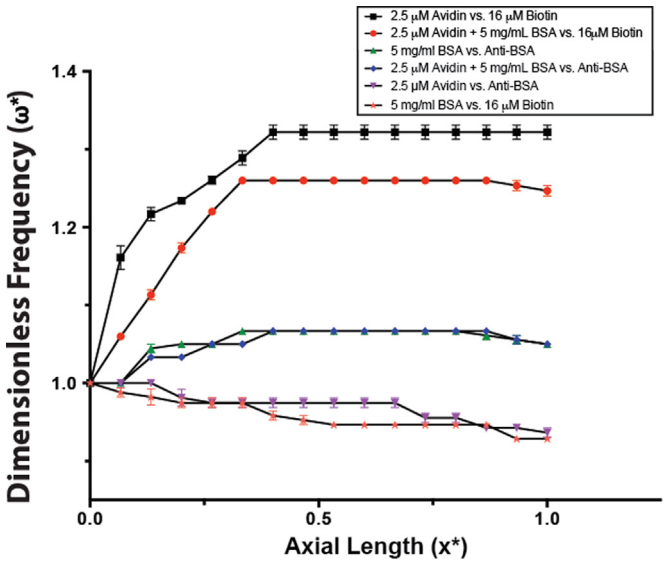

Fig. 5. IET sensorgram illustrating selective sensor response to both BSA/anti-BSA and avidin/biotin binding.

(Avrameas, 1992) between BSA and the surrounding biomolecules in solution could be influencing the interfacial conductivity and total concentration of avidin available for binding. However, as shown in the BSA sensorgram in Fig. 5, the addition of background avidin to the BSA solution during binding with anti-BSA does not affect the magnitude of the sensorgram. This suggests that non-specific interactions between BSA and avidin are minimal.

Because the sensor COF is driven by a combination of both target–receptor binding and interfacial smoothening by ionic diffusion, we speculate that the addition of BSA hinders the rate of avidin diffusion towards and across the interface, which slows the rate of the binding and leads to a lower sensor COF. Finally, it is worth noting that the reaction between BSA and anti-BSA does not produce the same change in COF when compared to the avidin and biotin reaction. We hypothesize this difference is due to the difference in binding kinetics between these two reactions. In comparing the K_d of each reaction, 10^{-15} and 10^{-4}, for the avidin–biotin and BSA–anti-BSA (Kausaite et al., 2007) reaction, respectively, the reaction between BSA and anti-BSA occurs at a slower rate than that of avidin and biotin. Since the reaction time is slower, binding requires a longer distance down the axial length of the microchannel. Because the diffusion of ions across the electrical interface is constantly occurring and decreasing the interfacial conductivity, the reaction requiring a greater length scale must compete with an ever-decreasing interfacial conductivity, which ultimately leads to a smaller magnitude in the change of COF. Future work will focus on developing a better understanding of these physicochemical mechanisms that link species reaction and diffusional rates with interfacial conductivity in order to better optimize sensor response.

3.4. Label-free femtomolar detection in BSA

We next performed a series of experiments to determine the IET sensor's limit of detection (LOD) and how the IE performs as a transducer against an abundant background protein (5 mg/mL BSA). The IET biosensor response was measured as a function of avidin concentration, ranging from 50 fM to 2.5 μM, both with and without BSA. Fig. 6 shows a series of sensorgrams for avidin–biotin binding at the EI (Fig. 6a) and with a BSA background (Fig. 6b). The net IET sensor response increases with avidin concentration, and eventually levels to a constant value some distance down the electrode array. The eventual leveling of the IET signal at a given position down the array length can be attributed to the saturation of the interface with bound avidin–biotin complex; avidin is

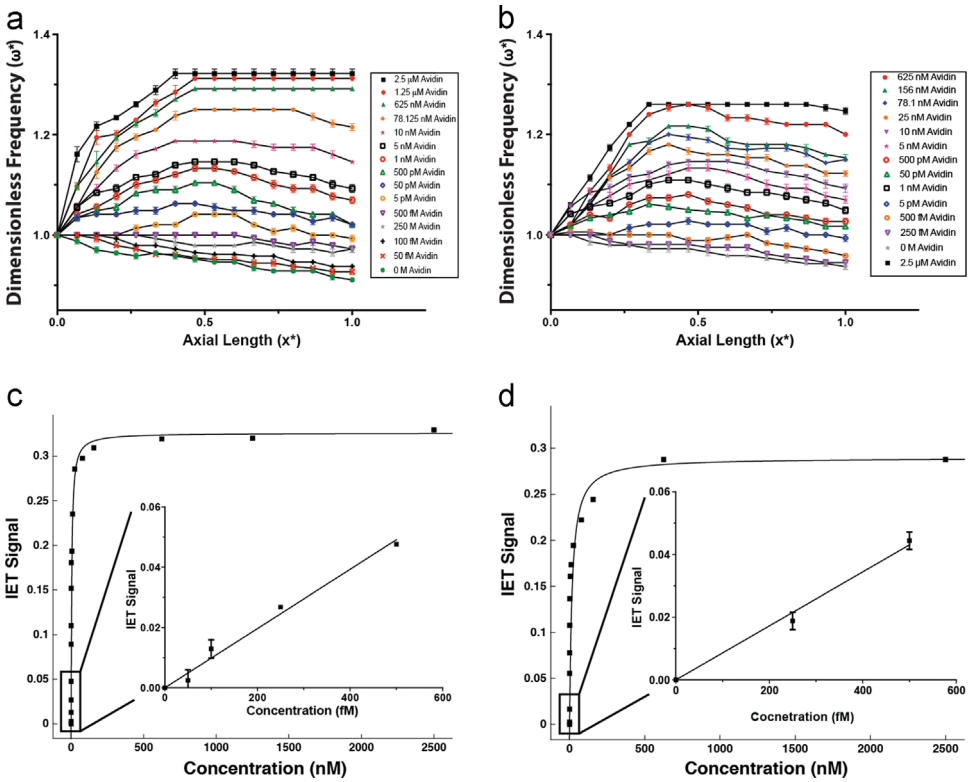

Fig. 6. (A) IET sensorgram of increasing concentrations of avidin; (B) sensorgram illustrating sensor response against a background of serum albumin; (C) sensor binding curve showing IET limit of detection without a BSA background; and (D) with a BSA background.

depleted from the local EI and the sensor response saturates.

The magnitude of each saturated sensorgram response at a fixed distance down the electrode array ($x^*=0.5$) was isolated and plotted as a function of avidin concentration. The resulting calibration curve is shown in Fig. 6c for an EI without BSA and in Fig. 6d for the interface subjected to a serum background. For each analytical curve, the sensor exhibits a linear response with increasing concentrations of avidin up to 500 fM, as shown in the subplots of each (Fig. 6c and d). Beyond this linear concentration range, the sensor deviates and begins to level off, eventually saturating at an avidin concentration at approximately 1 μM. The concentration LOD was calculated using the 3-sigma method ($S/N=3$) for each binding curve. Without background BSA, the sensor LOD was 209 fM, while the addition of BSA decreased sensor sensitivity with a corresponding LOD of 626 fM.

4. Conclusions

In this work, we presented a sensitive and selective label-free electrokinetic biosensor for detecting biomolecules at electrically polarizable liquid interfaces. Biomolecular binding occurs at the diffuse electrical interface formed between two co-flowing microfluidic laminar streams with different electrical properties. The biosensor approach is based on measuring the electrical field-induced displacement frequency response of this interface, which is sensitively influenced by specific biomolecular binding. In this manner, the biosensor design utilizes this interface as substrate for biomolecular binding, and its motion in an electric field as a signal transducer. We have shown that binding increases the electrical conductivity at the interface, which is transduced as a change in interfacial frequency response, and forms the basis for our presented interfacial electrokinetic transduction (IET) method. The system developed can detect low femtomolar avidin concentrations against a 5 mg/mL background of serum albumin, and can be reconfigured to detect other proteins. The IET sensor has the potential be extended to other biomolecular systems for the detection of disease biomarkers in serum and urine. Furthermore, because binding occurs dynamically in time over the length of the microchannel interface, it should be possible to use this IET approach to study the binding kinetics of a variety of specific ligand–receptor pairs. Finally, while fluorescent microscopy was used in this work to measure interface position, future work will focus on developing inexpensive methods for measuring interface displacement electrically, extending our IET approach to more complex samples such as whole blood and urine, reducing interfacial diffusion of the electric interface, and developing reactive transport models to study binding kinetics at the liquid interface.

Acknowledgments

This work was supported by an NSF CAREER Award, CBET-1351253 and CBET-1511185.

References

Ariyaratne, A., Zocchi, G., 2015. Plasmon resonance enhanced mechanical detection of ligand binding. Appl. Phys. Lett. 106, 013702. http://dx.doi.org/10.1063/1.4905550.

Atencia, J., Beebe, D.J., 2005. Controlled microfluidic interfaces. Nature 437, 648–655. http://dx.doi.org/10.1038/nature04163.

Avrameas, S., 1992. Amplification systems in immunoenzymatic techniques. J. Immunol. Methods 150, 23–32. http://dx.doi.org/10.1016/0022-1759(92)90062-X.

Cao, L., Cheng, L., Zhang, Z., Wang, Y., Zhang, X., Chen, H., Liu, B., Zhang, S., Kong, J., 2012. Visual and high-throughput detection of cancer cells using a graphene oxide-based FRET aptasensing microfluidic chip. Lab Chip 12, 4864–4869. http://dx.doi.org/10.1039/C2LC40564D.

Coltro, W.K.T., Neves, R.D.S., Motheo, A.D.J., da Silva, J.A.F., Carrilho, E., 2014. Microfluidic devices with integrated dual-capacitively coupled contactless conductivity detection to monitor binding events in real time. Sens. Actuators B: Chem. 192, 239–246. http://dx.doi.org/10.1016/j.snb.2013.10.114.

Cooper, M.A., Cooper, M.A., 2002. Optical biosensors in drug discovery. Nat. Rev. Drug Discov. 1, 515–528. http://dx.doi.org/10.1038/nrd838.

Desmond, M., Mavrogiannis, N., Gagnon, Z., 2012. Maxwell–Wagner polarization and frequency-dependent injection at aqueous electrical interfaces. Phys. Rev. Lett. 109, 187602.

Dong, C., Ren, J., 2014. Coupling of fluorescence correlation spectroscopy with capillary and microchannel analytical systems and its applications. Electrophoresis 35, 2267–2278. http://dx.doi.org/10.1002/elps.201300648.

Fu, X., Mavrogiannis, N., Doria, S., Gagnon, Z., 2015. Microfluidic pumping, routing and metering by contactless metal-based electro-osmosis. Lab Chip . http://dx.doi.org/10.1039/C5LC00504C.

Gagnon, Z., Mazur, J., Chang, H.-C., 2010a. Integrated AC electrokinetic cell separation in a closed-loop device. Lab Chip 10, 718–726. http://dx.doi.org/10.1039/b917220c.

Gagnon, Z., Senapati, S., Chang, H.-C., 2010b. Optimized DNA hybridization detection on nanocolloidal particles by dielectrophoresis. Electrophoresis 31, 666–671. http://dx.doi.org/10.1002/elps.200900473.

Giraud, G., Schulze, H., Li, D.-U., Bachmann, T.T., Crain, J., Tyndall, D., Richardson, J., Walker, R., Stoppa, D., Charbon, E., Henderson, R., Arlt, J., 2010. Fluorescence lifetime biosensing with DNA microarrays and a CMOS-SPAD imager. Biomed. Opt. Express 1, 1302–1308. http://dx.doi.org/10.1364/BOE.1.001302.

Hatch, A., Garcia, E., Yager, P., 2004. Diffusion-based analysis of molecular interactions in microfluidic devices. Proc. IEEE 92, 126–139. http://dx.doi.org/10.1109/JPROC.2003.820547.

Hatch, A., Kamholz, A.E., Hawkins, K.R., Munson, M.S., Schilling, E.A., Weigl, B.H., Yager, P., 2001. A rapid diffusion immunoassay in a T-sensor. Nat. Biotechnol. 19, 461–465. http://dx.doi.org/10.1038/88135.

Ismagilov, R.F., Stroock, A.D., Kenis, P.J.A., Whitesides, G., Stone, H.A., 2000. Experimental and theoretical scaling laws for transverse diffusive broadening in two-phase laminar flows in microchannels. Appl. Phys. Lett. 76, 2376–2378. http://dx.doi.org/10.1063/1.126351.

Kamholz, A.E., Weigl, B.H., Finlayson, B.A., Yager, P., 1999. Quantitative analysis of molecular interaction in a microfluidic channel: the T-sensor. Anal. Chem. 71, 5340–5347. http://dx.doi.org/10.1021/ac990504j.

Kausaite, A., van Dijk, M., Castrop, J., Ramanaviciene, A., Baltrus, J.P., Acaite, J., Ramanavicius, A., 2007. Surface plasmon resonance label-free monitoring of antibody antigen interactions in real time. Biochem. Mol. Biol. Educ. 35, 57–63. http://dx.doi.org/10.1002/bmb.22.

Lee, H., Sun, E., Ham, D., Weissleder, R., 2008. Chip–NMR biosensor for detection and molecular analysis of cells. Nat. Med. 14, 869–874. http://dx.doi.org/10.1038/nm.1711.

Lee, Y.-K., Deval, J., Tabeling, P., Ho, C.-M., 2001. Chaotic mixing in electrokinetically and pressure driven micro flows. MEMSYS-01, 483–486. http://dx.doi.org/10.1109/MEMSYS.2001.906584.

Lin, M.X., Hyun, K.-A., Moon, H.-S., Sim, T.S., Lee, J.-G., Park, J.C., Lee, S.S., Jung, H.-I., 2013. Continuous labeling of circulating tumor cells with microbeads using a vortex micromixer for highly selective isolation. Biosens. Bioelectron. 40, 63–67. http://dx.doi.org/10.1016/j.bios.2012.06.016.

Mavrogiannis, N., Desmond, M., Gagnon, Z.R., 2015. Fluidic dielectrophoresis: the polarization and displacement of electrical liquid interfaces. Electrophoresis . http://dx.doi.org/10.1002/elps.201400454.

Mavrogiannis, N., Desmond, M., Gagnon, Z.R., 2014. Fluidic dielectrophoresis: the polarization and displacement of electrical liquid interfaces. Electrophoresis . http://dx.doi.org/10.1002/elps.201400454.

Myszka, D.G., Rich, R.L., 2000. Implementing surface plasmon resonance biosensors in drug discovery. Pharm. Sci. Technol. Today 3, 310–317. http://dx.doi.org/10.1016/S1461-5347(00)00288-1.

Palchetti, I., Mascini, M., 2008. Nucleic acid biosensors for environmental pollution monitoring. Analyst 133, 846–854. http://dx.doi.org/10.1039/B802920M.

Peruski, A.H., Johnson III, L.H., Peruski Jr., L.F., 2002. Rapid and sensitive detection of biological warfare agents using time-resolved fluorescence assays. J. Immunol. Methods 263, 35–41. http://dx.doi.org/10.1016/S0022-1759(02)00030-3.

Peruski, A.H., Peruski, L.F., 2003. Immunological methods for detection and identification of infectious disease and biological warfare agents. Clin. Diagn. Lab. Immunol. 10, 506–513. http://dx.doi.org/10.1128/CDLI.10.4.506-513.2003.

Pohl, H.A., 1951. The motion and precipitation of suspensoids in divergent electric fields. J. Appl. Phys. 22, 869–871. http://dx.doi.org/10.1063/1.1700065.

Pollet, J., Delport, F., Janssen, K.P.F., Jans, K., Maes, G., Pfeiffer, H., Wevers, M., Lammertyn, J., 2009. Fiber optic SPR biosensing of DNA hybridization and DNA–protein interactions. Biosens. Bioelectron. 25, 864–869. http://dx.doi.org/10.1016/j.bios.2009.08.045.

Rebe Raz, S., Haasnoot, W., 2011. Multiplex bioanalytical methods for food and environmental monitoring. Trends Anal. Chem. 30, 1526–1537. http://dx.doi.org/10.1016/j.trac.2011.04.016.

Rodriguez, M.C., Kawde, A.-N., Wang, J., 2005. Aptamer biosensor for label-free impedance spectroscopy detection of proteins based on recognition-induced switching of the surface charge. Chem. Commun. 0, 4267–4269. http://dx.doi.org/10.1039/B506571B.

Roelse, M., de Ruijter, N.C.A., Vrouwe, E.X., Jongsma, M.A., 2013. A generic microfluidic biosensor of G protein-coupled receptor activation – monitoring cytoplasmic [Ca2+] changes in human HEK293 cells. Biosens. Bioelectron. 47,

436–444. http://dx.doi.org/10.1016/j.bios.2013.03.065.
Voura, E.B., Jaiswal, J.K., Mattoussi, H., Simon, S.M., 2004. Tracking metastatic tumor cell extravasation with quantum dot nanocrystals and fluorescence emission-scanning microscopy. Nat. Med. 10, 993–998. http://dx.doi.org/10.1038/nm1096.
Wan, Y., Su, Y., Zhu, X., Liu, G., Fan, C., 2013. Development of electrochemical immunosensors towards point of care diagnostics. Biosens. Bioelectron. 47, 1–11. http://dx.doi.org/10.1016/j.bios.2013.02.045.
Wang, J., 2006. Electrochemical biosensors: towards point-of-care cancer diagnostics. Biosens. Bioelectron. 21, 1887–1892. http://dx.doi.org/10.1016/j.bios.2005.10.027.
Watkins, N.N., Hassan, U., Damhorst, G., Ni, H., Vaid, A., Rodriguez, W., Bashir, R., 2013. Microfluidic CD4+ and CD8+ T lymphocyte counters for point-of-care HIV diagnostics using whole blood. Sci. Transl. Med. 5. http://dx.doi.org/10.1126/scitranslmed.3006870 214ra170–214ra170.
Yoo, J.-C., La, G.-S., Kang, C.J., Kim, Y.-S., 2008. Microfabricated polydimethylsiloxane microfluidic system including micropump and microvalve for integrated biosensor. Curr. Appl. Phys. 8, 692–695. http://dx.doi.org/10.1016/j.cap.2007.04.050.
Yoo, J.H., Woo, D.H., Chang, M.-S., Chun, M.-S., 2014. Microfluidic based biosensing for *Escherichia coli* detection by embedding antimicrobial peptide-labeled beads. Sens. Actuators B: Chem. 191, 211–218. http://dx.doi.org/10.1016/j.snb.2013.09.105.